Materials Science & Engineering A 615 (2014) 231–239

Contents lists available at ScienceDirect

Materials Science & Engineering A

journal homepage: www.elsevier.com/locate/msea

Effect of short-term annealing on the microstructures and flow properties of an Al–1% Mg alloy processed by high-pressure torsion

Olivier Andreau [a], Jenő Gubicza [b], Nian Xian Zhang [c], Yi Huang [c,*], Péter Jenei [b], Terence G. Langdon [c,d]

[a] Phelma – School of Engineering in Physics, Electronics and Materials, Grenoble INP Minatec, 3 Parvis Louis Neel, BP 257, 38016 Grenoble Cedex 1, France
[b] Department of Materials Physics, Eötvös Loránd University, Pázmány Péter s. 1/A, H-1117 Budapest, Hungary
[c] Materials Research Group, Faculty of Engineering and the Environment, University of Southampton, Southampton SO17 1BJ, UK
[d] Departments of Aerospace & Mechanical Engineering and Materials Science, University of Southern California, Los Angeles, CA 90089-1453, USA

ARTICLE INFO

Article history:
Received 7 May 2014
Received in revised form
7 July 2014
Accepted 8 July 2014
Available online 15 July 2014

Keywords:
Al–Mg alloy
Annealing
Hardness
High-pressure torsion
Portevin–Le Chatelier effect

ABSTRACT

An Al–1% Mg solid solution alloy with an annealed grain size of ~400 μm was processed by high-pressure torsion (HPT) to produce a grain size of ~200 nm with a high fraction of high-angle grain boundaries. Tensile testing at room temperature showed this material exhibited excellent strength but with little or no ductility. It is demonstrated that a combination of reasonable ductility and good strength may be achieved by subjecting samples to a short term anneal of 10 min following the HPT processing. Annealing at 423 K increased the average grain size to ~360 nm, reduced the overall strength to a value that was ~75% of the value without annealing but gave reasonable elongations of up to >0.2. Both the initial unprocessed Al–Mg alloy and the sample annealed after HPT exhibited serrated flow due to the Portevin–Le Chatelier (PLC) effect. The results suggest that the introduction of short-term annealing after HPT processing may be an effective and simple procedure for achieving a reasonable level of strength together with good ductility after processing by HPT.

1. Introduction

The processing of metals through the application of severe plastic deformation (SPD) is now an established procedure for producing bulk fully-dense solids with ultrafine-grained (UFG) structures and grain sizes within the submicrometer or nanometre ranges [1]. Two SPD methods currently receiving considerable attention are equal-channel angular pressing (ECAP) [2] and high-pressure torsion (HPT) [3]. After SPD processing, it was established that UFG metals have highly deformed microstructures with high dislocation densities within the grains [4] and with high-energy non-equilibrium grain boundaries containing an excess of extrinsic dislocations [5,6].

Generally, UFG metals exhibit high strength but their ductility is limited because they have both a low rate of strain hardening and a low strain rate sensitivity [7,8]. Several techniques have been proposed to improve the ductility after SPD processing and one method is to subject the processed material to a short-term anneal. This procedure has the potential of ordering the defect structures within the grain boundaries and thereby producing more equilibrated grain boundaries without incurring any significant grain growth. Reports are available showing the general validity of this approach for Cu processed by ECAP [9], commercial purity Ti processed by ECAP and drawing [10] and ECAP—Conform and drawing [11], Ti processed by HPT [12] and a Ti–6Al–4V alloy processed by ECAP—Conform and extrusion [13].

The present investigation was initiated in order to determine the effect of short-term anneals of 10 min on the microstructures and room temperature mechanical properties of a UFG Al–1% Mg solid solution alloy processed by HPT. This alloy was selected because there is only limited information on the processing of this alloy by HPT but it is well established that the alloy exhibits excellent grain refinement, with grain sizes of <500 nm, when processed by ECAP [14,15].

2. Experimental material and procedures

An Al–1.0% Mg solid solution alloy was used in this study with the composition given in wt% (equivalent to Al–1.1 at% Mg). The material was received in the form of extruded rods having diameters of 13 mm and, prior to any machining, these rods were annealed for 1 h at 773 K to give an average initial grain size of ~400 μm. After annealing, the rods were machined to reduce the

* Corresponding author.
E-mail address: y.huang@soton.ac.uk (Y. Huang).

http://dx.doi.org/10.1016/j.msea.2014.07.018
0921-5093/

diameters to 9.85 mm and then sliced into discs with thicknesses of ~1.2 mm. These sliced discs were ground with abrasive papers to final thicknesses of ~0.8 mm and then processed by HPT at room temperature under quasi-constrained conditions [16,17] through total numbers of turns, *N*, of 1/4, 1/2, 1, 3, 5 and 10. The HPT processing was conducted as described in an earlier report [18] except that an MoS_2 lubricant was not placed around each disc on the upper and lower anvils prior to processing. The HPT was performed using an imposed pressure of 6.0 GPa and a rotational speed for the lower anvil of 1 rpm. Following HPT, some of the samples processed through the maximum of 10 turns were selected for short term annealing in a vacuum for 10 min at the relatively low temperatures of 373, 423, 473 and 523 K.

Both the HPT-processed discs and the post-HPT annealed discs were carefully ground with abrasive paper in order to remove layers of ~0.1 mm thickness from the disc surfaces. The samples were then polished on cloth with diamond paste; a final polishing was performed using a colloidal silica solution and the distorted surface layer with a thickness of several micrometres was removed by Ar ion milling. The grain structures in the HPT-processed and the post-HPT annealed specimens were examined near the edges of the discs by electron back-scattered diffraction (EBSD) using a FEI Quanta 3D scanning electron microscope (SEM). For the initial annealed and unprocessed material, the microstructure was examined using a JSM6500F thermal field emission SEM coupled with EBSD.

The microstructures of the Al–1Mg samples were also studied at the peripheries of the HPT-processed discs using X-ray line profile analysis. The X-ray line profiles were measured using a high-resolution rotating anode diffractometer (type: RA-MultiMax9, manufacturer: Rigaku) using $CuK\alpha_1$ (λ=0.15406 nm) radiation. Two-dimensional imaging plates detected the Debye–Scherrer diffraction rings. The line profiles were determined as the intensity distributions perpendicular to the rings which were obtained by integrating the two-dimensional intensity distributions along the rings. The line profiles were then evaluated using extended Convolutional Multiple Whole Profile (eCMWP) analysis [19,20].

The Vickers microhardness, Hv, was measured on polished mirror-like disc surfaces using an FM300 microhardness tester equipped with a Vickers indenter. Each hardness measurement used a load of 100 gf and a dwell time of 15 s. These measurements were taken at positions along the disc diameters separated by incremental distances of 0.3 mm and with the average hardness at each position estimated from four individual points recorded around the selected position and separated by distances of 0.15 mm. These measurements were used to provide the variations of hardness across each disc together with the associated error bars recorded at the 95% level.

Tensile specimens were cut from three different sets of samples: from annealed and unprocessed samples, from samples processed by 10 turns of HPT and from samples processed through 10 turns of HPT and then subjected to post-HPT annealing treatments at 423, 473 or 523 K. To avoid any problems associated with the occurrence of microstructural inhomogeneities in the centres of the discs, these tensile specimens were prepared using electro-discharge machining where two separate specimens were cut from each disc and these specimens were placed symmetrically on either side of the centre of the disc with the central point of each sample located at 2 mm from the disc centre [21]. All tensile specimens were pulled to failure at room temperature using an Instron testing machine operating at a constant rate of

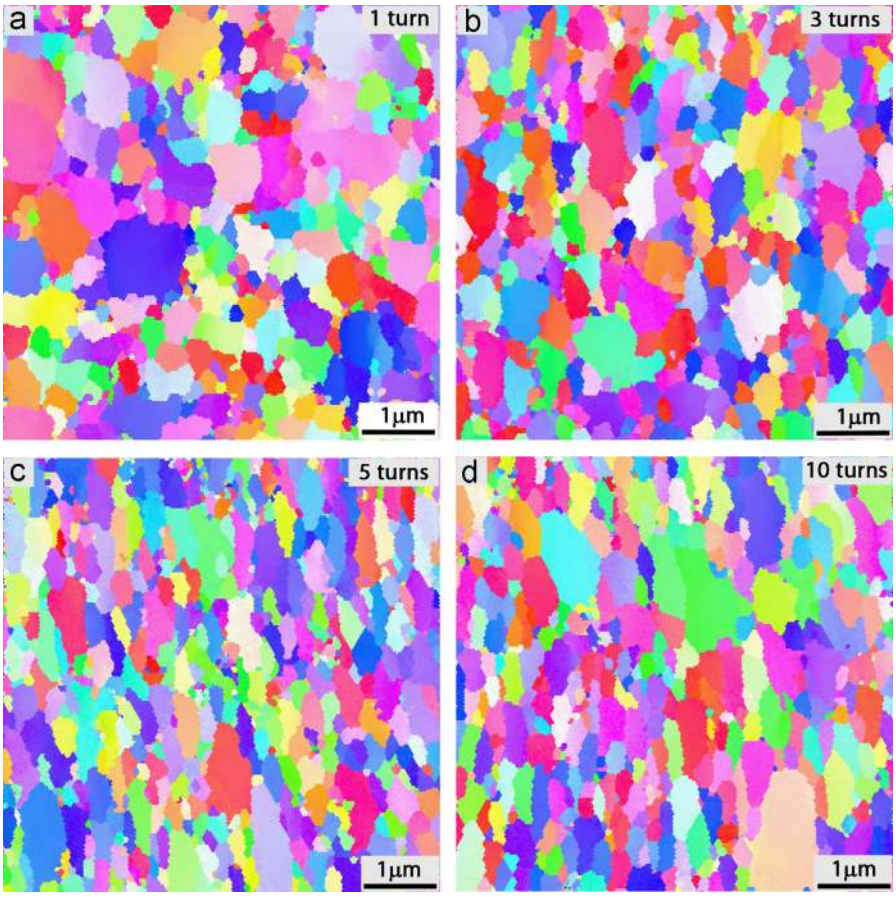

Fig. 1. Microstructures after HPT processing through (a) 1, (b) 3, (c) 5 and (d) 10 turns.

cross-head displacement with initial strain rates of 1.0×10^{-4}, 1.0×10^{-3} and $1.0\times10^{-2}\,s^{-1}$.

3. Experimental results

3.1. The grain structure and grain boundary misorientation evolution during HPT

Typical EBSD images are shown in Fig. 1 taken near the edges of the discs for samples processed by HPT through (a) 1, (b) 3, (c) 5 and (d) 10 turns. To provide comprehensive microstructural information, the corresponding distributions for the measured grain sizes are shown in Fig. 2 for the same numbers of turns. Thus, there is very significant grain refinement even after 1 turn of HPT where the grain size has been reduced from an initial value of ~400 μm to a value of ~240 nm in Fig. 2(a). After 3 turns there is little or no additional grain refinement in Fig. 1(b) but the grains are beginning to show an elongated configuration and the average size is again ~240 nm in Fig. 2(b). Further torsional straining to 5 turns leads to very clear grain elongation and a smaller average grain size of ~200 nm. Finally, after 10 turns there are some relatively coarse grains within the elongated microstructure as in Fig. 1(d) and this leads to a larger average grain size of ~230 nm. This transition through grain refinement in the early stages to the later development of some limited coarse grains is supported by the grain size histograms shown in Fig. 2.

The distributions of the grain boundary misorientations are given in Fig. 3 after HPT through (a) 1, (b) 3, (c) 5 and (d) 10 turns where misorientation angles $>15^\circ$ are taken as high-angle boundaries and the solid curves represent the statistical prediction for a set of random orientations [22,23]. After 1 turn of HPT there is a very high fraction of ~80% of high-angle boundaries and this fraction increases slightly to ~85% after 5 turns and then decreases again to ~80% after 10 turns. Since these fractions are sufficiently similar it is reasonable to conclude that there is no significant change with increasing numbers of turns in HPT. Furthermore, as with pure Al [24] and with the same Al–1% Mg alloy [25] processed by ECAP, the theoretical distribution is not fully attained because there is an excess of boundaries having low angles of misorientation. This is generally attributed to the large numbers of dislocations and the associated development of new low-angle boundaries that continue throughout processing by HPT or ECAP.

3.2. The hardness evolution during HPT

The evolution in hardness with increasing numbers of HPT turns is shown in Fig. 4 where the lower dashed line corresponds to the initial hardness of Hv ≈ 37 in the annealed material and experimental points are shown for the hardness values across the discs after processing from 1/4 to 10 turns. Inspection shows that after 1/4, 1/2 and 1 turn the hardness values increase significantly around the edges of each disc but there are smaller increases near the centres. This is consistent with the expectations for HPT processing because the equivalent von Mises strain, ε_{eq}, imposed on the disc is given by the relationship [26]:

$$\varepsilon_{eq}=\frac{2\pi Nr}{h\sqrt{3}} \tag{1}$$

where r is the radial distance from the centre of the disc and h is the initial height (or thickness) of the disc. It follows from Eq. (1)

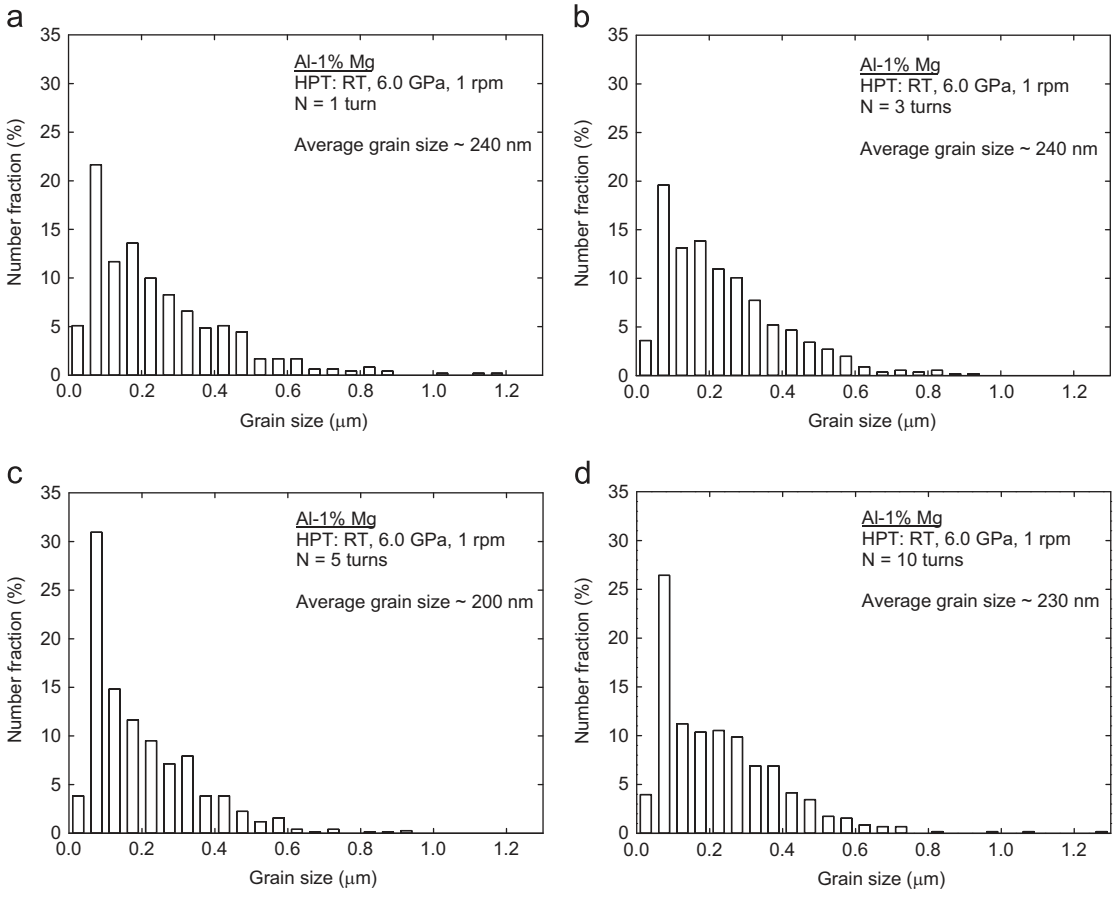

Fig. 2. Grain size distributions after HPT processing through (a) 1, (b) 3, (c) 5 and (d) 10 turns.

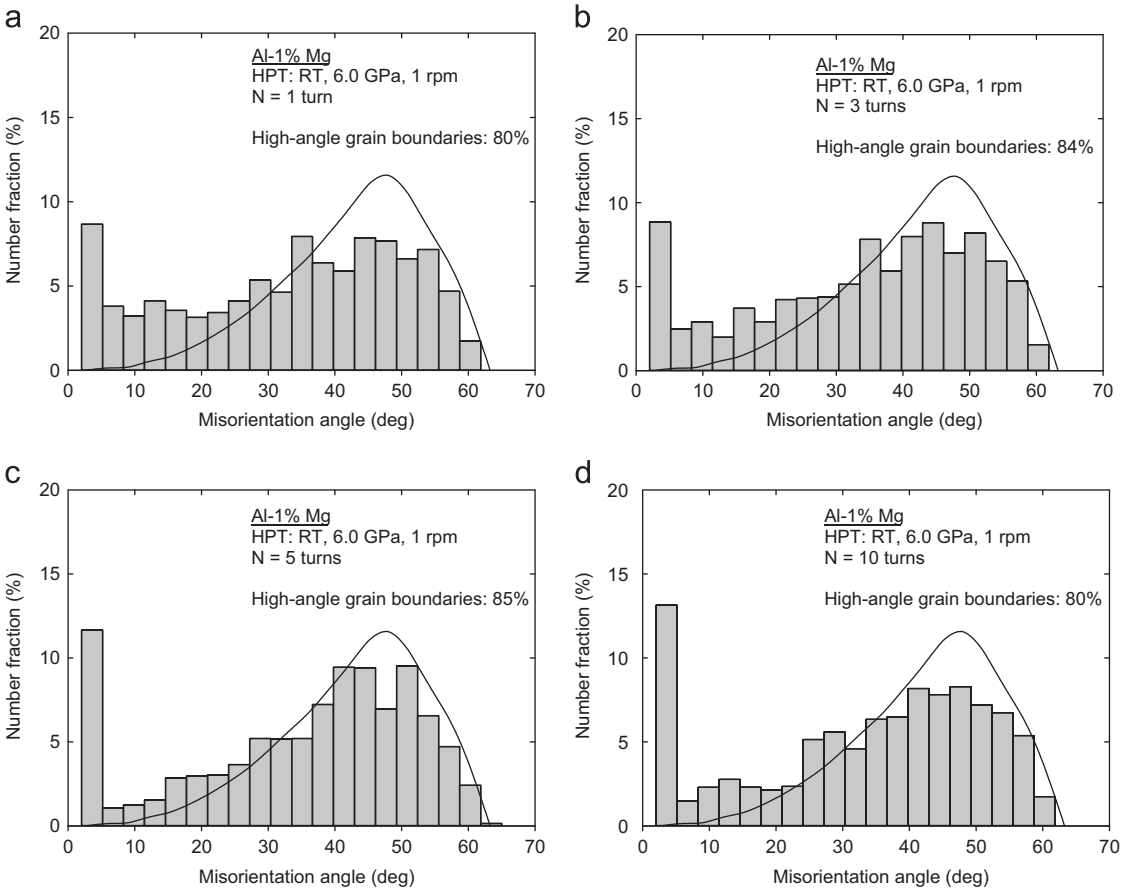

Fig. 3. Misorientation distributions after HPT processing through (a) 1, (b) 3, (c) 5 and (d) 10 turns.

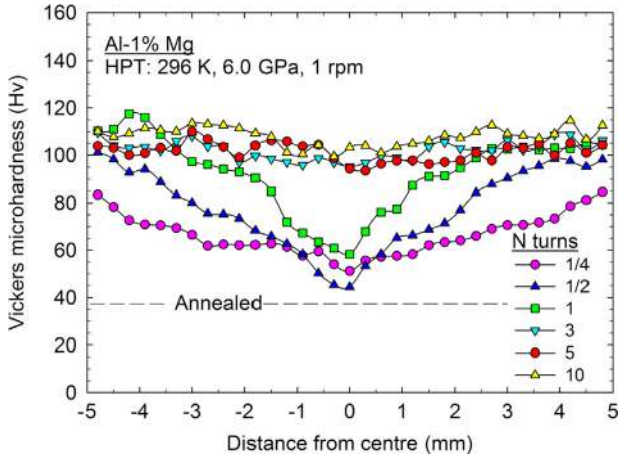

Fig. 4. Distribution of Vickers microhardness, Hv, along the diameters of discs processed by HPT through 1/4. 1/2, 1, 3, 5 and 10 turns.

that the strain has a maximum value at the outer edge of the disc and it is equal to zero at the centre of the disc where $r=0$.

It is also apparent that after 3, 5 and 10 turns the hardness values appear to be reasonably homogeneous across the disc diameters so that the values have reached an essentially stable condition. This follows the prediction of strain gradient plasticity modelling which shows that the hardness values will gradually evolve with increasing torsional straining in HPT processing towards an essentially uniform distribution [27]. In practice, close inspection of Fig. 4 shows that the hardness values recorded after 10 turns are slightly larger than after 3 and 5 turns.

3.3. The evolution of microhardness and grain structure after the post-HPT annealing treatment

In order to investigate the effect of a short post-HPT annealing treatment, samples processed through 10 turns of HPT were annealed for 10 min at selected constant temperatures from 373 to 523 K. Fig. 5 shows the microstructures developed after annealing at (a) 373, (b) 423, (c) 473 and (d) 523 K where (a) and (b) have the same magnification as in Fig. 1 but (c) and (d) have a lower magnification. The microstructure after annealing at 373 K looks very similar to the microstructure shown in Fig. 1(d) after 10 turns of HPT and the grains again have an elongated appearance with an average grain size of ~210 nm. After annealing at 423 K, the grains in Fig. 5(b) have a bi-modal distribution with some very fine grains and some coarser grains and the grain morphology is now reasonably equiaxed with an average grain size of ~360 nm. This shows that recrystallisation occurs when conducting short-term annealing at a temperature of 423 K. Further increasing the annealing temperatures to 473 and 523 K leads to reasonably equiaxed grains but the average grain sizes increase to ~0.94 and ~1.98 μm, respectively.

The overall microhardness values and the variations in the grain size following the post-HPT annealing are summarised in Fig. 6 where a short-term anneal at 373 K retains the same microhardness and grain size as at room temperature (296 K) but at higher annealing temperatures of 423, 473 and 523 K the microhardness values decrease and the average grain sizes increase. The incremental increase in grain size in Fig. 6 becomes larger with increasing annealing temperature and this is consistent with earlier reports where similar alloys were processed by ECAP and then annealed for 1 h in order to evaluate their thermal stability [15,28,29].

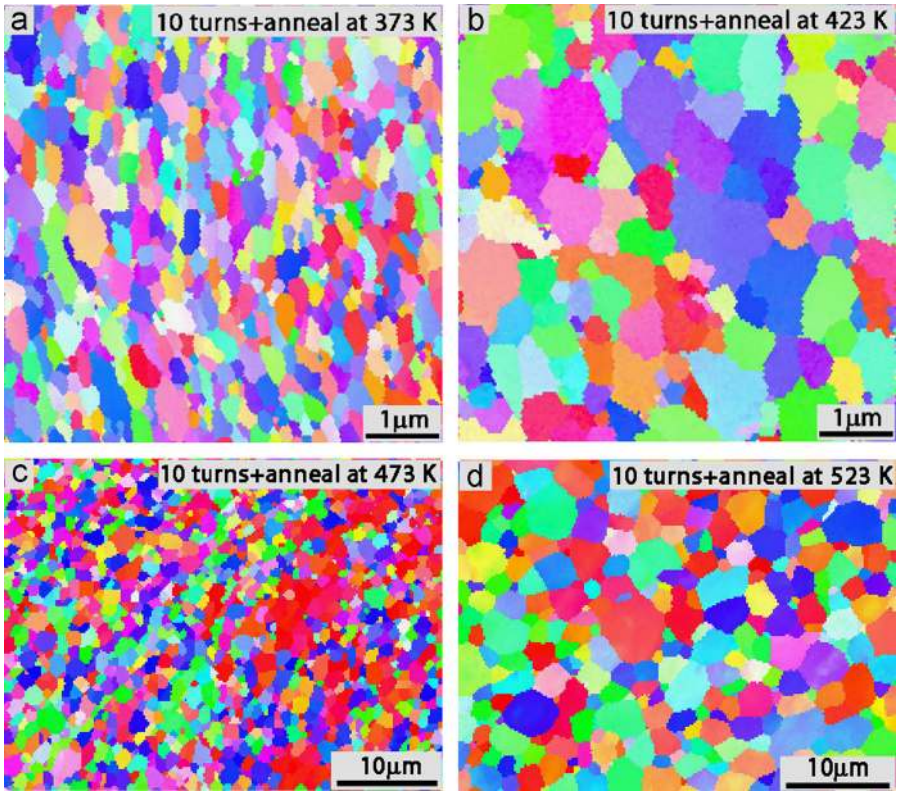

Fig. 5. Microstructures after HPT processing through 10 turns and annealing for 10 min at (a) 373, (b) 423, (c) 473 and (d) 523 K.

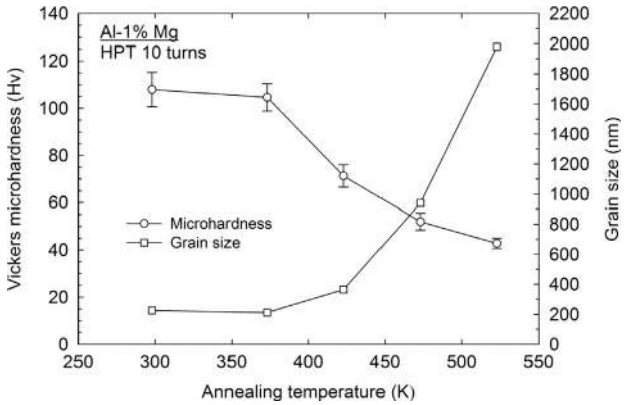

Fig. 6. Variation of the microhardness and grain size with the post-HPT annealing temperature.

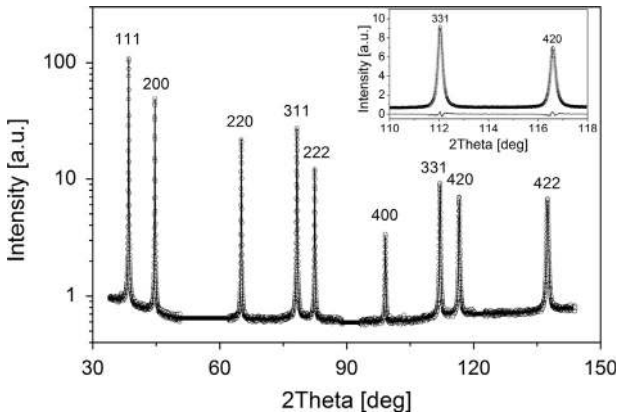

Fig. 7. The eCMWP fitting of the sample processed through 10 revolutions of HPT: the open circles and the solid line represent the measured data and the fitted curves, respectively.

3.4. *Microstructural results from the X-ray line profile analysis both with and without post-HPT annealing*

In the line profile evaluation method using the extended Convolutional Multiple Whole Profile (eCMWP) analysis [19,20], the diffraction pattern is fitted by the sum of a background spline and the convolution of the instrumental pattern and the theoretical line profiles are then related to the crystallite size and the densities of dislocations and twins. As an example, Fig. 7 shows the fitting for the sample processed by 10 revolutions of HPT without post-HPT annealing. The area-weighted mean crystallite size, $\langle x \rangle_{area}$, is calculated from the median and the variance of the crystallite size distribution as $\langle x \rangle_{area} = m \exp(2.5\sigma^2)$. The twin boundary probability corresponds to the relative frequency of twin boundaries among the {111} lattice planes and this was below the detection limit in the present investigation. The area-weighted mean crystallite size and the dislocation density, ρ, were then determined from the analysis and the results are summarised in Table 1 for samples processed through 1, 3, 5 and 10 turns and after 10 turns of HPT and then post-HPT annealing at 373 and 423 K.

Table 1
Parameters for the microstructure obtained by X-ray line profile analysis: $\langle x \rangle_{area}$ is the area-weighted mean crystallite size and ρ is the dislocation density.

HPT sample: value of N	$\langle x \rangle_{area}$ (nm)	ρ (10^{14} m^{-2})
1	123 ± 13	4.0 ± 0.5
3	116 ± 12	3.5 ± 0.4
5	114 ± 13	3.8 ± 0.4
10	117 ± 13	3.7 ± 0.4
10 + anneal at 373 K	116 ± 12	3.5 ± 0.5
10 + anneal at 423 K	208 ± 23	0.5 ± 0.1

These calculations show that the crystallite size and the dislocation density are saturated at the edges of the discs even after the first revolution of HPT. Furthermore, the measured dislocation density is similar to the value reported after 8 passes of ECAP at room temperature [30]. In the present experiments both the crystallite size and the dislocation density remain essentially unchanged during the annealing treatment at 373 K but annealing at 423 K increases the crystallite size by a factor of about two and decreases the dislocation density by about one order of magnitude. For samples annealed at higher temperatures, the crystallite size and the dislocation density were higher and lower, respectively, than the detection limits of the present X-ray line profile analysis.

3.5. The tensile properties with and without post-HPT annealing

The objective of the post-HPT annealing treatment was to evaluate the potential for influencing the strain hardening rate and the flow stress in tensile testing at room temperature. The results from the tensile tests are shown in Fig. 8 for the three initial strain rates of (a) 1.0×10^{-4}, (b) 1.0×10^{-3} and (c) $1.0 \times 10^{-2}\,s^{-1}$. Separate plots are shown in Fig. 8 for the annealed and unprocessed material, samples processed through 10 turns of HPT without post-HPT annealing and samples processed by HPT for 10 turns and annealed at 423, 473 and 523 K. Inspection shows that the initial unprocessed samples consistently exhibit the largest elongations to failure and the lowest flow stresses.

It is apparent from Fig. 8 that the specimens processed by 10 turns without post-HPT annealing exhibit both the highest stresses and very small elongations before failure at all strain rates. By contrast, samples subjected to post-HPT annealing at 473 and 523 K display higher elongation but at significantly lower stress levels. It appears that annealing for 10 min at 423 K gives high flow stresses that are inherited from the HPT processing but at the same time there is a significant improvement in the elongation to failure compared with the sample not subjected to post-HPT annealing. The advantage of the short post-HPT annealing is clearly demonstrated in Fig. 8(b) and (c) at the two faster strain rates where the samples processed by HPT exhibited brittle behaviour and broke before yielding but a post-HPT annealing treatment for only 10 min decreased the strength by $<25\%$ but gave reasonable elongations to failure with engineering strains of >0.2. Inspection of all tensile stress–strain curves in Fig. 8 shows that the post-HPT short anneal leads consistently to a decreasing strength and increasing elongation with increasing annealing temperature. In general, post-HPT annealing at a temperature of 423 K appears to be the optimum condition for attaining reasonable strength coupled with reasonable ductility.

3.6. Evidence for serrated flow and the Portevin–Le Chatelier effect

It is now well established that many alloys exhibit serrated yielding in tensile testing where the stress fluctuates around the mean value in a regular and periodic manner. This behaviour, which is known as the Portevin–Le Chatelier (PLC) effect, arises when moving dislocations are held up and periodically break away from their solute atom atmospheres. There are now numerous reports documenting the occurrence of the PLC effect in dilute Al–Mg alloys [31–39] and it is reasonable to anticipate the occurrence of this effect in the present investigation because it

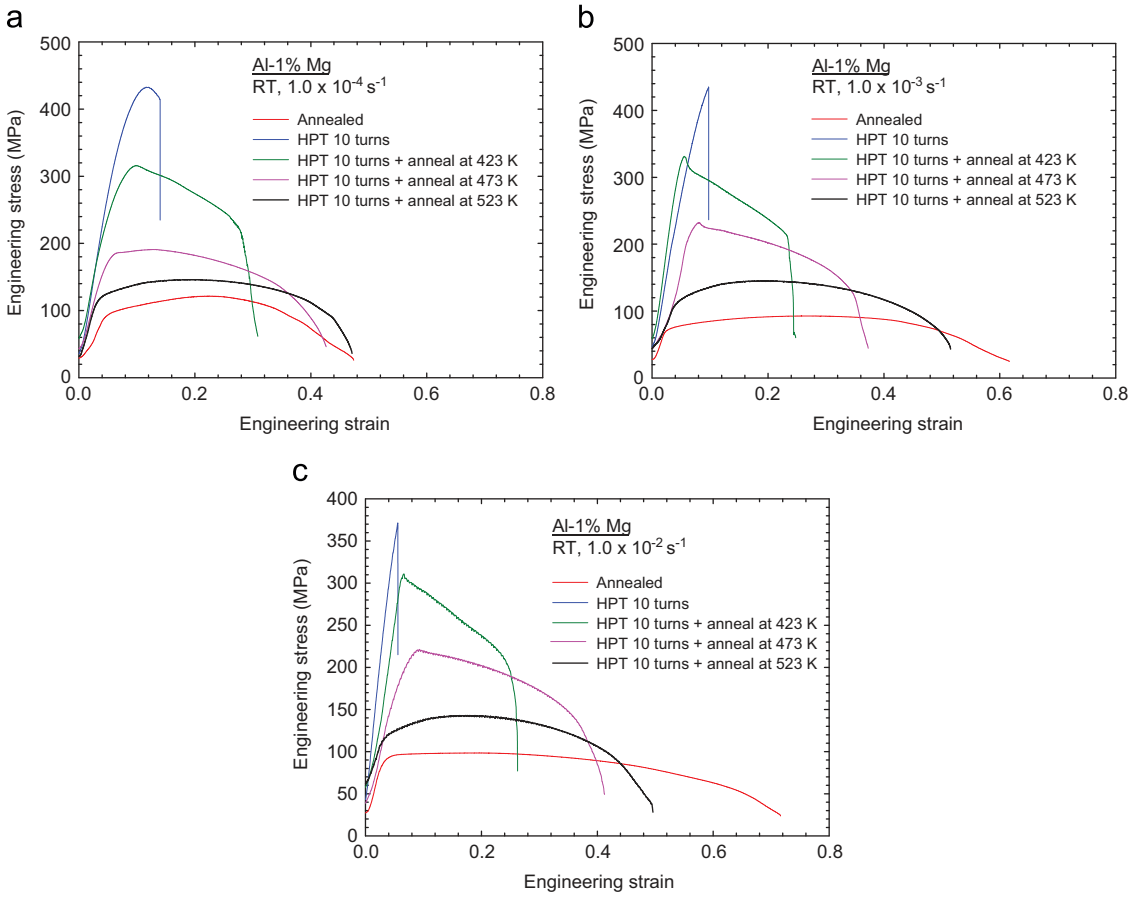

Fig. 8. Stress–strain curves at room temperature for the annealed material, after HPT through 10 turns and after HPT through 10 turns and annealing at 423, 473 and 523 K at (a) 1.0×10^{-4}, (b) 1.0×10^{-3} and $1.0 \times 10^{-2}\,s^{-1}$ respectively.

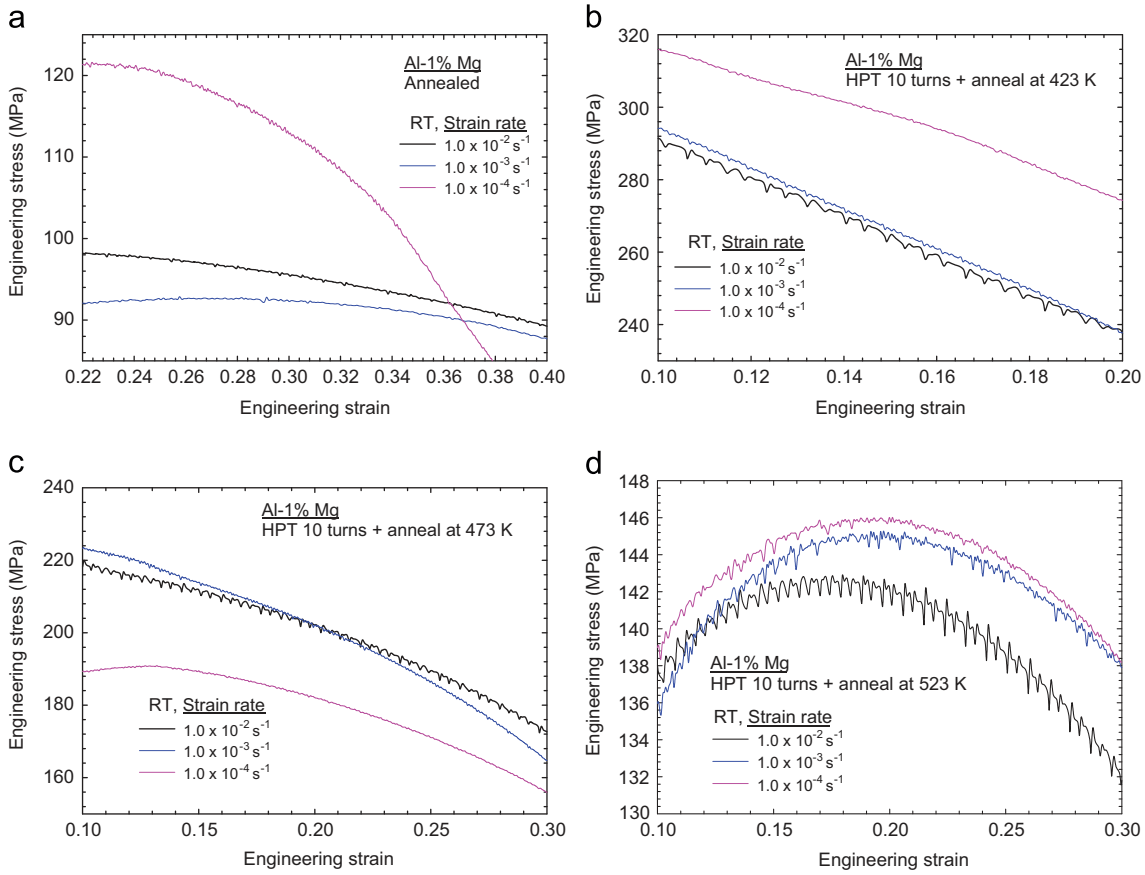

Fig. 9. Examples of serrated yielding in sections of the stress–strain curves for (a) the annealed material and after HPT through 10 turns and annealing at (b) 423, (c) 473 and (d) 523 K.

has been shown that the amplitudes of the serrations become larger when the grain size is reduced [31]. Accordingly, a very careful inspection in Fig. 8 shows evidence for the PLC effect in both the unprocessed annealed samples and the samples subjected to a short post-HPT annealing treatment and the presence of serrations may be readily demonstrated by replotting portions of the stress–strain curves over short increments of the engineering strains. These plots are presented in Fig. 9 where separate curves for the three testing strain rates are shown for (a) the annealed but unprocessed samples and for samples processed by HPT and then subjected to post-HPT annealing at (b) 423, (c) 473 and (d) 523 K. All these curves exhibit serrated flow but the effect becomes especially apparent at the fastest strain rate in Fig. 9(d).

Different types of serrations are generally identified in materials exhibiting the PLC effect depending upon the testing strain rate and the nature of the serrations including whether they are continuous or discontinuous and whether they rise above or drop below the general level of the stress–strain curve [32,40–42]. In normal flow, the flow stress increases with the applied strain rate so that the strain rate sensitivity is positive but in serrated flow, because of the dynamic interactions between the mobile dislocations and solute atoms, the strain rate sensitivity may become negative in some restricted ranges of temperature, strain and strain rate in the process known as dynamic strain aging (DSA) [37,39,42]. There is clear evidence for the occurrence of DSA in the present investigation in Fig. 9(b) and (d) where the stress decreases with increasing strain rate.

Before HPT processing the annealed samples display the PLC effect at all three strain rates in Fig. 9(a) but the magnitudes of the serrations tend to become more obvious at the slowest strain rate of $1.0 \times 10^{-4}\,s^{-1}$. By contrast, for samples subjected to a post-HPT annealing it is evident from Fig. 9(b)–(d) that the serrations become more obvious in tests conducted at the fastest strain rate of $1.0 \times 10^{-2}\,s^{-1}$. The transition from more evident PLC at the slowest strain rate in the unprocessed samples to the fastest strain rate in the samples given a post-HPT annealing treatment is related to the magnitude of the dislocation density and the grain size. The unprocessed samples were annealed at 773 K for 1 h so that they have a low initial dislocation density and the Mg atoms are in solution. The strain rate regime of the PLC effect is determined by the rate of Mg lattice diffusion in Al: at very low strain rates Mg atoms can follow dislocations without serrated flow while at higher rates the moving dislocations periodically break away from the solute atom atmospheres. At very high strain rates, the diffusion of solute atoms is too slow to give serrated flow.

In SPD-processed samples, the PLC effect is usually not observed due to the distributions of solute atoms among the large densities of dislocations and grain boundaries. However, in the samples subjected to HPT plus a post-HPT annealing treatment, the HPT processing introduces a high dislocation density but the subsequent short-term annealing increases the average grain size as shown in Fig. 6 and, as documented in Table 1, the dislocation density is reduced so that the structure becomes more equilibrated and serrated flow occurs again. The strain rate regime of the PLC effect in the post-HPT annealed specimens is thereby shifted to higher values compared to the unprocessed sample due to the faster diffusion of Mg atoms along the dislocations and grain boundaries that remain after annealing.

4. Discussion

Exceptional grain refinement was achieved in an Al–1% Mg alloy having an initial grain size of ~400 μm. Processing by HPT at room temperature using an applied pressure of 6.0 GPa led to an

average grain size of ~200 nm after 5 turns. This grain size is smaller by a factor of two than the mean grain size of ~450 nm which was reported for the same alloy after processing by ECAP through 6 passes at room temperature [14]. After 5 turns of HPT there was also a high fraction of ~85% of high-angle grain boundaries and this is even higher than the fraction of ~65% reported for the same alloy after processing at room temperature through 8 passes of ECAP [25]. The present results establish, therefore, that there is excellent grain refinement in the Al–1% Mg alloy through processing by HPT.

Despite the success in achieving a highly-refined microstructure, it is readily apparent from Fig. 8 that the tensile properties of the HPT-processed specimens are not satisfactory when testing at room temperature. The curves shown in Fig. 8(a–c) for the material processed by HPT through 10 turns display excellent strength up to > 400 MPa at the two lowest strain rates but with little or no ductility: specifically, there is only a very small elongation before failure at the slowest strain rate of $1.0 \times 10^{-4}\,s^{-1}$ and at the two faster strain rates the samples exhibit brittle behaviour.

Imposing a short term anneal of 10 min after the HPT processing has a significant effect on the microstructure as shown in Fig. 5 and summarised graphically in Fig. 6. Thus, whereas an anneal at 373 K has little effect, there is a minor increase in grain size and a measurable decrease in the hardness after annealing at 423 K and at even higher annealing temperatures the average grain sizes increase rapidly up to and above ~1 μm and the values of the hardness are also decreased. The relevant stress–strain curves in Fig. 8 for the samples processed by HPT and then subjected to short term annealing provide a very clear demonstration of the advantage of imposing a short term anneal on this alloy. For an anneal of 10 min at 423 K the average grain size increased to ~360 nm, the overall strength was reduced to about 75% of the value without annealing and the stress–strain curves exhibited reasonable elongations up to > 0.2. Even higher elongations were achieved when annealing at the higher temperatures but there was also a considerable reduction in the overall strength. These results suggest there is an optimum condition for the Al–1% Mg alloy by processing using HPT at room temperature and then giving the material a short anneal for 10 min at 423 K.

The values of the Vickers microhardness shown in Fig. 4 are typical of those recorded in many other alloys. In an early investigation of HPT it was proposed that the various experimental points in a plot such as Fig. 4 may be effectively brought together onto a single curve by plotting each point in the form of the measured value of Hv against the equivalent strain calculated using Eq. (1) [43]. This approach has been used in many recent reports [44–50] and the same plot is shown in Fig. 10 based on the experimental points recorded in the present investigation. This plot confirms that the hardness of the Al–1% Mg alloy stabilizes at Hv ≈ 110.

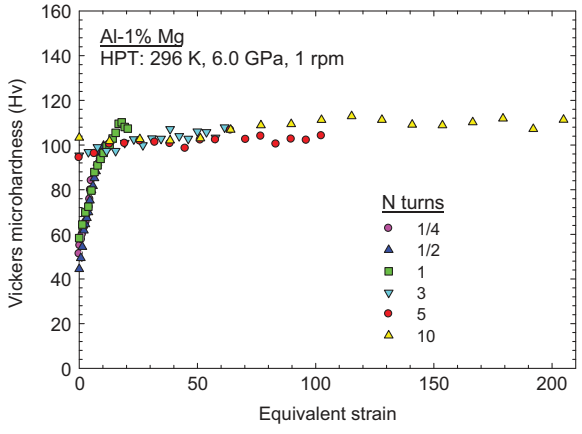

Fig. 10. Values of the Vickers microhardness plotted as a function of the equivalent strain in discs processed by HPT through 1/4, 1/2, 1, 3, 5 and 10 turns.

Plots of the type shown in Fig. 10 are designated hardening without recovery [51] and they are representative of a large number of metals including various aluminium alloys [52–56], copper alloys [57–60], magnesium alloys [61,62] and the Ti–6Al–4V alloy [63,64]. However, the results are different from high purity Al where the high stacking fault energy leads to rapid recovery by cross-slip at the edges of the discs so that initially, in the early stages of HPT processing, higher values of hardness are recorded in the centres of the discs [65,66]. This latter behaviour is generally designated hardening with recovery [51]. The similarities between the hardness behaviour and the grain refinement characteristics of the Al–1% Mg alloy and many other alloys suggest, therefore, that the same approach of a short term anneal after HPT processing may have a general validity as a simple procedure for achieving reasonable strength and good ductility in UFG metals processed by HPT.

5. Summary and conclusions

1. Experiments were conducted on an Al–1% Mg solid solution alloy to evaluate the effect of introducing a short term anneal following HPT processing. This alloy had an initial annealed grain size of ~400 μm which was refined to ~200 nm with a high fraction of high-angle grain boundaries through processing by HPT at room temperature.
2. In the as-processed condition, the material exhibited excellent strength but little or no ductility when testing in tension at room temperature. The introduction of short anneals for 10 min following the HPT processing led to a small reduction in strength but a significant increase in ductility.
3. The optimum annealing condition was identified as an anneal for 10 min at a temperature of 423 K where the grain size increased to ~360 nm, the strength was reduced to ~75% of the value in the as-processed condition and there was a reasonable ductility with elongations up to > 0.2. It is suggested that short term annealing after HPT processing may be an effective and simple procedure in many metals for achieving both good strength and reasonable levels of ductility.

Acknowledgement

This work was supported by the European Research Council under ERC Grant agreement no. 267464-SPDMETALS and by the Hungarian Scientific Research Fund, OTKA, Grant no. K-109021.

References

[1] T.G. Langdon, Acta Mater. 61 (2013) 7035.
[2] R.Z. Valiev, T.G. Langdon, Prog. Mater. Sci. 51 (2006) 881.
[3] A.P. Zhilyaev, T.G. Langdon, Prog. Mater. Sci. 53 (2008) 893.
[4] J. Wang, Z. Horita, M. Furukawa, M. Nemoto, N.K. Tsenev, R.Z. Valiev, Y. Ma, T.G. Langdon, J. Mater. Res. 8 (1993) 2810.
[5] Z. Horita, D.J. Smith, M. Furukawa, M. Nemoto, R.Z. Valiev, T.G. Langdon, J. Mater. Res. 11 (1996) 1880.
[6] Z. Horita, D.J. Smith, M. Nemoto, R.Z. Valiev, T.G. Langdon, J. Mater. Res. 13 (1998) 446.
[7] R. Valiev, Nature 419 (2002) 887.
[8] R. Valiev, Nat. Mater. 3 (2004) 511.
[9] T. Suo, Y.L. Li, F. Zhao, Q. Deng, K. Xie, Mater. Res. Innov. 15 (s1) (2011) S69.
[10] I. Semenova, G. Salimgareeva, G. Da Costa, W. Lefebvre, R. Valiev, Adv. Eng. Mater. 12 (2010) 803.
[11] A.V. Polyakov, I.P. Semenova, R.Z. Valiev, Y. Huang, T.G. Langdon, MRS Commun. 3 (2013) 249.
[12] R.Z. Valiev, A.V. Sergueeva, A.K. Mukherjee, Scr. Mater. 49 (2003) 669.

[13] A.V. Polyakov, I.P. Semenova, Y. Huang, R.Z. Valiev, T.G. Langdon, Adv. Eng. Mater. 16 (2014) 1038. http://dx.doi.org/10.1002/adem.201300530.
[14] Y. Iwahashi, M. Nemoto, Z. Horita, T.G. Langdon, Metall. Mater. Trans. A 29A (1998) 2503.
[15] H. Hasegawa, S. Komura, A. Utsunomiya, Z. Horita, M. Furukawa, M. Nemoto, T.G. Langdon, Mater. Sci. Eng. A 265 (1999) 188.
[16] R.B. Figueiredo, P.R. Cetlin, T.G. Langdon, Mater. Sci. Eng. A 528 (2011) 8198.
[17] R.B. Figueiredo, P.H.R. Pereira, M.T.P. Aguilar, P.R. Cetlin, T.G. Langdon, Acta Mater. 60 (2012) 3190.
[18] M. Kawasaki, T.G. Langdon, Mater. Sci. Eng. A 498 (2008) 341.
[19] G. Ribárik, J. Gubicza, T. Ungár, Mater. Sci. Eng. A 387–389 (2004) 343.
[20] L. Balogh, G. Ribárik, T. Ungár, J. Appl. Phys. 100 (2006) 023512.
[21] A. Loucif, R.B. Figueiredo, M. Kawasaki, T. Baudin, F. Brisset, R. Chemam, T.G. Langdon, J. Mater. Sci. 47 (2012) 7815.
[22] J.K. Mackenzie, M.J. Thomson, Biometrika 44 (1957) 205.
[23] J.K. Mackenzie, Biometrika 45 (1958) 229.
[24] M. Kawasaki, Z. Horita, T.G. Langdon, Mater. Sci. Eng. A 524 (2009) 143.
[25] C. Xu, Z. Horita, T.G. Langdon, Mater. Sci. Eng. A 528 (2011) 6059.
[26] R.Z. Valiev, Yu.V. Ivanisenko, E.F. Rauch, B. Baudelet, Acta Mater. 44 (1996) 4705.
[27] Y. Estrin, A. Molotnikov, C.H.J. Davies, R. Lapovok, J. Mech. Phys. Solids 56 (2008) 1186.
[28] K. Oh-ishi, Z. Horita, D.J. Smith, R.Z. Valiev, M. Nemoto, T.G. Langdon, J. Mater. Res. 14 (1999) 4200.
[29] Z. Horita, T. Fujinami, M. Nemoto, T.G. Langdon, Metall. Mater. Trans. A 31A (2000) 691.
[30] J. Gubicza, N.Q. Chinh, Gy. Krállics, I. Schiller, T. Ungár, Curr. Appl. Phys. 6 (2006) 194.
[31] H. Fujita, T. Tabata, Acta Metall. 25 (1977) 793.
[32] G.G. Saha, P.G. McCormick, P. Rama Rao, Mater. Sci. Eng. 62 (1984) 187.
[33] J.M. Robinson, M.P. Shaw, Mater. Sci. Eng. 174A (1994) 1.
[34] J.M. Reed, M.E. Walter, Mater. Sci. Eng. A 359 (2003) 1.
[35] B.Q. Han, Z. Lee, S.R. Nutt, E.J. Lavernia, F.A. Mohamed, Metall. Mater. Trans. A 34A (2003) 603.
[36] F.B. Klose, A. Ziegenbein, F. Hagemann, H. Neuhäuser, P. Hähner, M. Abbadi, A. Zeghloul, Mater. Sci. Eng. A 369 (2004) 76.
[37] G.J. Fan, G.Y. Wang, H. Choo, P.K. Liaw, Y.S. Park, B.Q. Han, E.J. Lavernia, Scr. Mater. 52 (2005) 929.
[38] E. Samuel, J.J. Jonas, F.H. Samuel, Metall. Mater. Trans. A 42A (2011) 1028.
[39] L. Ziani, S. Boudrahem, H. Ait-Amokhtar, M. Mehenni, B. Kedjar, Mater. Sci. Eng. A 536 (2012) 239.
[40] T.G. Langdon, F.A. Mohamed, Scr. Metall. 7 (1973) 1199.
[41] F.A. Mohamed, K.L. Murty, T.G. Langdon, Acta Metall. 22 (1974) 325.
[42] C. Fressengeas, A.J. Beaudoin, M. Lebyodkin, L.P. Kubin, Y. Estrin, Mater. Sci. Eng. A 400–401 (2005) 226.
[43] A. Vorhauer, R. Pippan, Scr. Mater. 51 (2004) 921.
[44] K. Edalati, T. Fujioka, Z. Horita, Mater. Sci. Eng. A 497 (2008) 168.
[45] Y. Harai, K. Edalati, Z. Horita, T.G. Langdon, Acta Mater. 57 (2009) 1147.
[46] K. Edalati, Y. Ito, K. Suehiro, Z. Horita, Int. J. Mater. Res. 100 (2009) 1668.
[47] K. Edalati, T. Fujioka, Z. Horita, Mater. Trans. 50 (2009) 44.
[48] K. Edalati, Z. Horita, Mater. Trans. 51 (2010) 1051.
[49] K. Edalati, Z. Horita, Mater. Sci. Eng. A 528 (2011) 7514.
[50] S. Lee, Z. Horita, Mater. Trans. 53 (2012) 38.
[51] M. Kawasaki, J. Mater. Sci. 49 (2014) 18.
[52] A. Loucif, R.B. Figueiredo, T. Baudin, F. Brisset, T.G. Langdon, Mater. Sci. Eng. A 527 (2011) 4864.
[53] A. Loucif, R.B. Figueiredo, T. Baudin, F. Brisset, R. Chemam, T.G. Langdon, Mater. Sci. Eng. A 532 (2012) 139.
[54] Y. Huang, R.B. Figueiredo, T. Baudin, F. Brisset, T.G. Langdon, Adv. Eng. Mater. 14 (2012) 1018.
[55] Y. Huang, R.B. Figueiredo, T. Baudin, A.L. Helbert, F. Brisset, T.G. Langdon, J. Mater. Sci. 47 (2012) 7796.
[56] S. Sabbaghianrad, T.G. Langdon, Mater. Sci. Eng. A 596 (2014) 52.
[57] Y.Z. Tian, S.D. Wu, Z.F. Zhang, R.B. Figueiredo, N. Gao, T.G. Langdon, Acta Mater. 59 (2011) 2783.
[58] Y.Z. Tian, S.D. Wu, Z.F. Zhang, R.B. Figueiredo, N. Gao, T.G. Langdon, Scr. Mater. 65 (2011) 477.
[59] X.H. An, Q.Y. Liu, S.D. Wu, Z.F. Zhang, R.B. Figueiredo, N. Gao, T.G. Langdon, Philos. Mag. 91 (2011) 3307.
[60] Y.Z. Tian, Z.F. Zhang, T.G. Langdon, J. Mater. Sci. 48 (2013) 4606.
[61] A. Al-Zubaydi, R.B. Figueiredo, Y. Huang, T.G. Langdon, J. Mater. Sci. 48 (2013) 4661.
[62] M. Kawasaki, R.B. Figueiredo, Y. Huang, T.G. Langdon, J. Mater. Sci. 49 (2014) 6586. http://dx.doi.org/10.1007/s10853-014-8262-8.
[63] Y.C. Wang, T.G. Langdon, Mater. Sci. Eng. A 559 (2013) 861.
[64] Y.C. Wang, T.G. Langdon, J. Mater. Sci. 48 (2013) 4646.
[65] C. Xu, Z. Horita, T.G. Langdon, Acta Mater. 55 (2007) 203.
[66] C. Xu, Z. Horita, T.G. Langdon, Mater. Trans. 51 (2010) 2.